



Steady flows of constant-viscosity viscoelastic fluids in a planar T-junction



H.M. Matos, P.J. Oliveira *

Departamento de Engenharia Electromecânica, Universidade da Beira Interior, Rua Marques D'Avila e Bolama, 6201-001 Covilhã, Portugal¹

ARTICLE INFO

Article history:

Received 24 August 2013

Received in revised form 23 August 2014

Accepted 25 August 2014

Available online 3 September 2014

Keywords:

T-junction flow

Non-Newtonian fluid

Viscoelastic effects

FENE-CR and FENE-MCR models

Hemodynamics

Vascular diseases

ABSTRACT

The study reported in this paper is based on computational fluid dynamics simulations of steady viscoelastic flows through a planar two-dimensional T-junction. The purpose of this study is to analyse the influence of constitutive model and fluid elasticity upon the main recirculating flow characteristics formed at the junction and the shear stress fields.

The fluid here considered has some characteristics similar to blood which makes the study relevant to hemodynamics. By taking into account some fluid complexities, such as inherent viscoelasticity, which is shown to affect flow recirculation and in particular the shear stress distribution, the study gives a contribution to fundamental issues in the genesis of vascular diseases.

We restrict attention in this study to steady state flows and analyse the influence of elastic effects, either by varying the Deborah number or by increasing the dispersed phase elasticity-inducing concentration parameter and extensibility. In these steady simulations we apply either the FENE-CR or the FENE-MCR constitutive models, which are based on the non-linear finite extensibility dumbbell model but assume different simplifications in the derivation of the respective differential model equations. Those simplifications were assumed to be only important in unsteady flows but the present results show that Lagrangian acceleration in steady-state flow do also lead to significant differences.

© 2014 Elsevier B.V. All rights reserved.

1. Introduction

Viscoelastic flows through T-junctions are relevant to hemodynamics and micro fluid dynamics, in addition to other macro engineering applications where the viscoelasticity of the binary fluid/flow set may be of relevance.

Our motivation is mainly connected to the fact that atherosclerotic plaque formation tends to occur in artery walls near blood vessel bifurcations and a large part of the review that follows discusses some aspects of this difficult and on-going scientific matter. Basically we highlight two points: flow recirculation in bifurcations is a key factor in atherosclerosis; blood is viscoelastic, and viscoelasticity alters recirculating flow characteristics, but that has often been neglected. Fluid mixing in micro devices, when many fluids show strong viscoelasticity effects due to the small dimensions involved, is also a potential beneficial of the present fundamental study. We however emphasize from the outset that even if hemodynamics has been a main motivation, the work so far is a general contribution to viscoelastic flow effects in a 90° T-junction geometry.

Hemodynamics is essential to understanding atherosclerosis, the most common cardiovascular pathology, which tends to be localized at sites of branching and arterial curvature [1], where regions of highly complex flow are found, with separation and recirculation, exhibiting both low mean shear stress [2] and reversal flow [3]. Blood is a suspension of multiple components, of which red blood cells are the most predominant [e.g. 4,5] being responsible for the non-Newtonian properties of blood: shear-thinning, thixotropy and viscoelasticity [6] (the review by Owens [7] is highly recommended).

In hemodynamical studies, viscoelastic fluid effects are usually neglected. For blood flows in large arteries the Newtonian fluid approximation is widely used, see e.g. [4,7] and also [8], who mentions that non-Newtonian effects might be important in the smallest vessels; the consideration of non-Newtonian character usually boils down to a viscous GNF approach, see e.g. Gijzen et al. [9,10] who dealt with blood analog fluids in modelled arterial configurations (bends and carotid bifurcation). Numerical works in the hemodynamical field that take into account viscoelastic effects are scarce, one of the earliest was the work of Phillips and Deutsch [11] who employed a four constant Oldroyd-B model to represent unsteady pulsating flow in a straight axi-symmetric artery. Another very recent study using the same model was presented by Ikbāl et al. [12]. Works with

* Corresponding author.

E-mail addresses: heldermiguelmm@hotmail.com (H.M. Matos), pjpo@ubi.pt (P.J. Oliveira).

¹ Research Units: UMTF and CMAST, Covilhã and CEFT, Porto.

higher level of complexity of the constitutive model have been developed for example by Yeleswarapu et al. [13], Leuprecht and Perktold [4], and Bodnár et al. [14], who used a generalization of the Oldroyd-B model including the shear thinning effect simultaneously. Owens [7] (and subsequent papers) developed a differential stress model for blood, with some level of sophistication, which tries to incorporate the three aspects of shear-thinning, thixotropy and viscoelasticity. Recently Chakraborty et al. [15] carried out a study where various constitutive models, namely the Oldroyd-B, the FENE-P and Owens [7] blood model, were examined.

T-junction flows related to hemodynamics applications in 2D geometries relevant to the present investigation have been the focus of experimental and numerical studies by Liepsch, Khodadadi and co-workers [16–19]. Both the geometrical data (channel sizes and flow rate ratios through the diverting channel) and the fluid data (density; viscosity) used in this, and other papers by the present authors [20,21], were directly based on those previous studies. In [20] the steady and unsteady Newtonian flow through a 2D planar T-junction was examined in detail; in [21], the corresponding flow of a GNF fluid with variable viscosity based on a Carreau-Yasuda model suitable for blood, was addressed. In these studies by our group, viscoelasticity of the fluid has not been considered, except in [22] where the purpose was to tune and improve the numerical aspects of the simulation programme.

In microfluidic applications, rectangular cross-section T-junctions are often used, usually with the purpose of promoting passive mixing between two streams and in this case the flow arrangement is that of an impacting T-junction (two straight inlets, one main outlet at 90°), see e.g. Soleymani et al. [23]. However, the dividing T-junction flow arrangement, akin to the one here addressed, is also applied for example for electrokinetic injection in microchips (e.g. Bianchi et al. [24]). In most of these studies the fluid is assumed to be either Newtonian [23–25] or GNF [26]; viscoelasticity only recently starts being considered [27]. In this latter case, knowledge on the effects of elasticity upon recirculating eddies formed by a dividing T-junction is missing in the scientific literature.

The present study aims to quantify the influence of elasticity, through the Deborah number and the concentration parameter, on the eddy characteristics and the shear stress fields for steady two-dimensional T-junction flows. Recirculation zones are analyzed in detail since they are characterized by having very low shear stresses, while in the boundary with the running flow high shear stresses tend to develop, thus leading to steep stress gradients and large local spatial oscillations. In addition to the shear stress field, the vortex lengths and vortex strengths are analysed as well. Two FENE type viscoelastic constitutive models are used: FENE-CR and FENE-MCR. Both models are nonlinear, since the spring that connects the two beads of the underlying dumbbell unit is non-Hookean and, additionally, it cannot be stretched indefinitely. However these models do not describe shear thinning viscosity thus allowing attention to be focused on the elastic influences. Restricting consideration to steady flows, elasticity was varied in two ways: either by increasing the Deborah number, from the Newtonian case ($De = 0$) up to a maximum value for which it was possible to achieve a converged numerical solution; or by varying the so-called viscosity ratio ($0.3 \leq \beta \leq 0.9$), or the extensibility parameter, at a constant value of the Deborah number. Numerical solutions were obtained for the two constitutive models referred to above, in order to assess their distinct properties under identical conditions.

2. Governing equations

This section describes the mathematical model and provides some justification for its choice. The continuity and momentum transfer equations governing the present incompressible, isothermal and laminar flows are written as:

$$\nabla \cdot \mathbf{u} = 0 \quad (1)$$

$$\frac{\partial \rho \mathbf{u}}{\partial t} + \nabla \cdot (\rho \mathbf{u} \mathbf{u}) = -\nabla p + \nabla \cdot \boldsymbol{\tau} \quad (2)$$

where \mathbf{u} is the velocity vector, p is the pressure, ρ is the fluid density and $\boldsymbol{\tau}$ is the total extra stress tensor. The viscoelastic fluids considered here are treated as an homogeneous two-phase liquid or a polymeric-like solution, for which the total extra stress tensor can be decomposed as the sum of a Newtonian contribution and a viscoelastic contribution from a dispersed phase:

$$\boldsymbol{\tau} = \boldsymbol{\tau}_N + \boldsymbol{\tau}_V \quad (3)$$

In general this decomposition can be done even if the fluid is not truly a polymer solution but shows viscoelasticity from the presence of a dispersed phase as it is the case of blood flow, for instance. The stress tensor for the Newtonian component follows the standard Newton law of viscosity, expressing a linear and explicit stress–strain rate relationship:

$$\boldsymbol{\tau}_N = 2\eta_N \mathbf{D} \quad (4)$$

where $\mathbf{D} = (\nabla \mathbf{u} + \nabla \mathbf{u}^T)/2$ is the rate-of-strain tensor and η_N the Newtonian viscosity.

For non-Newtonian viscoelastic fluids, τ_V is non-zero and an additional equation to express the evolution of the viscoelastic non-Newtonian contribution to the stress is needed. Two rheological constitutive models derived from the finitely-extendable nonlinear dumbbell theory (FENE [28]) have been chosen, guided by the fact that we do not wish a varying viscosity, the FENE-CR [29] and FENE-MCR [30] models. They are applied in the present simulations of viscoelastic flow through the planar T-junction; the FENE-MCR model is only used initially when the models are compared, while the FENE-CR model is used in most of the study. In the FENE-CR model proposed by Chilcot and Rallison [29], the fluid has a constant shear viscosity but shows shear-thinning in both the relaxation time and the first normal stress difference. The rheological constitutive equation is expressed by:

$$\boldsymbol{\tau}_V + \lambda \left(\frac{\nabla \boldsymbol{\tau}_V}{f(\boldsymbol{\tau}_V)} \right) = 2\eta_V \mathbf{D} \quad (5)$$

where λ is the relaxation time of the fluid at zero shear rate, η_V is the non-Newtonian contribution to the viscosity, the symbol ∇ denotes the Oldroyd upper convected derivative expressed by:

$$\frac{\nabla}{Dt} = \frac{D\boldsymbol{\tau}}{Dt} - (\nabla \mathbf{u}^T \cdot \boldsymbol{\tau} + \boldsymbol{\tau} \cdot \nabla \mathbf{u}) \quad (6)$$

and the function $f(\boldsymbol{\tau})$ is given by:

$$f(\boldsymbol{\tau}_V) = \frac{L^2 + (\lambda/\eta_V) Tr(\boldsymbol{\tau}_V)}{L^2 - 3} \quad (7)$$

In the last equation L^2 is the maximum extensibility of the dumbbells, a parameter of the model which is kept constant in most of the simulations ($L^2 = 100$), and $Tr(\boldsymbol{\tau}_V)$ represents the trace operator.

The FENE-MCR model or modified FENE-CR model proposed by Coates et al. [30] is achieved by adding the simplification $Df(\boldsymbol{\tau}_V)/Dt \approx 0$ to Eq. (5) which results in the following stress tensor relationship:

$$\boldsymbol{\tau}_V + \frac{\lambda}{f(\boldsymbol{\tau}_V)} \frac{\nabla}{Dt} \boldsymbol{\tau}_V = 2\eta_V \mathbf{D} \quad (8)$$

Both FENE-CR and FENE-MCR models give identical responses in simple steady shear and elongational flows. The only difference between the two models occurs in transient and strongly convective flows, where the term neglected in the FENE-MCR model

$(\mathbf{u} \cdot \nabla(1/f))$ may be significant. In the particular case of flow through diverging T-junctions, the recirculation zones promote high variable gradients in space and can induce relative differences between the solutions obtained with these two constitutive models, as will be shown.

The relevant dimensionless parameters in this work are:

- L^2 – the extensibility parameter of FENE-CR and FENE – MCR models (either constant, $L^2 = 100$, or varied parametrically); (9a)

- $\beta = \frac{\eta_N}{\eta_0}$ – the viscosity ratio,
 $\eta_0 = \eta_N + \eta_V$ (to be varied); (9b)

- $c = \frac{\eta_V}{\eta_N} = \frac{1 - \beta}{\beta}$ – the concentration parameter (related to β); (9c)

- $\chi = \frac{Q_3}{Q_1}$ – the flow rate ratio (kept constant, $\chi = 0.7$); (9d)

- $Re = \frac{\rho \bar{u}_1 H}{\eta_0}$ – the Reynolds number (kept constant, $Re = 102$); (9e)

- $De = \frac{\lambda \bar{u}_1}{H}$ – the Deborah number (to be varied). (9f)

In the definition of the Deborah and Reynolds numbers \bar{u}_1 is the average velocity at the inlet section and H is the channel height. Since the main interest of the study was focused on elastic effects, some of those parameters were kept constant as indicated above. The extensibility parameter in the rheological models was fixed at the typical value $L^2 = 100$ (e.g. [14,15]) in most of the cases, or varied around that base value, and the Reynolds number as $Re = 102$ (value used in previous studies with Newtonian flows typical of hemodynamical applications [16–21]; see Section 4). In the case of blood flows, β is probably a constant parameter, whose value is however not well defined. For other applications, it makes sense to vary β as a model parameter and see how it influences the main T-junction flow characteristics.

3. Numerical method

The solution of the governing equations was obtained with a finite-volume method which solves algebraic equations derived after discretizing in space and time the differential equations described in the last section. The finite-volume method ensures conservation of mass and momentum over the whole domain and requires less computer space and CPU time when compared with finite-element methods [31].

The systems of linearized algebraic equations resulting from the discretisation process are solved iteratively and sequentially using an adaptation of the SIMPLEC algorithm [32] taking due account of the viscoelastic nature of the flows, as described by Oliveira et al. [33], and employing the time marching approach of Issa and Oliveira [34], which is also useful in steady flows as an alternative to under-relaxation.

Coupling between pressure, velocity and the stress fields was addressed with the method of Oliveira et al. [33,35]. The last version of the coupling technique for the velocity and stress fields [22] allows us to obtain solutions for steady-state flow which are independent of the particular time step (Δt) value used.

The diffusion and pressure gradient terms in the governing equations are represented by central differences, while the convection terms are approximated by the high resolution scheme CUBI-

STA [36] having simultaneously good numerical accuracy and improved characteristics in terms of iterative convergence for viscoelastic flows, as demonstrated by Alves et al. [36].

Converged solutions for the time-marching advancing method were assumed when the normalized residuals for all variables fell below a prescribed relative tolerance of 10^{-5} .

4. Geometry and computational mesh

We consider a two-dimensional T-junction geometry shown schematically in Fig. 1 where some of the relevant dimensions and flow features are sketched. The geometry possesses a constant channel height of H and the coordinate axes are centred in the bifurcation zone. Flow enters from the left at $x = -3.5H$ (with volumetric rate Q_1) and leaves from the top exit (Q_3), in the vertical channel ($y = 20.5H$), and from the right exit (Q_2), in the horizontal channel ($x = 22.5H$). The channel lengths (L) should be sufficiently long for the outlet flows to become fully-developed. According to Shah and London's [37] the minimum lengths that ensure fully-developed Newtonian flows at the outlets are given by:

$$\frac{L}{H} = \frac{0.315}{0.068Re + 1} + 0.044Re \quad (10)$$

Although the validity of this expression is limited to Newtonian flows, it is still useful to obtain a first idea of the required geometry dimensions. The present simulations were carried out at constant inertia, by fixing the Reynolds number at $Re = 102$, the same value adopted as a base case in previous numerical works [20–22], in addition to the original experimental studies of Liepsch et al. [16] and Khodadadi et al. [18,19]. It is a common value often used in hemodynamical studies, e.g. Leuprecht and Perktold [4] chose $Re = 100$. From the definition of the Reynolds number (Eq. (9e)), for $Re = 102$ the mean velocity at the inlet is $\bar{u}_1 = 0.0745$ m/s, the fluid density is $\rho = 1150$ kg/m³ and the total fluid viscosity given by the sum of a Newtonian and a viscoelastic contribution is $\eta_0 = \eta_N + \eta_V = 0.0084$ Pa s (all dimensional quantities are based on the experiments of [18,19] in which $H = 0.01$ m; the fluid was a glycerine-water solution with a viscosity about the double of that of blood at high shear rates).

Shah and London's expression, Eq. (10), results in $L_2 = L_3 = 4.5H$ for $Re = 102$. However, in order to guarantee fully-developed flow conditions at the outlets and since Shah and London expression is restricted to Newtonian fluid, longer channel lengths were considered, namely $L_2 = 22H$ and $L_3 = 20H$ as in previous works [20–22]. In addition, the inlet duct length should also be long enough to ensure a fully-developed flow upstream the bifurcation zone, and for that we applied $L_1 = 3.0H$ following [17–19].

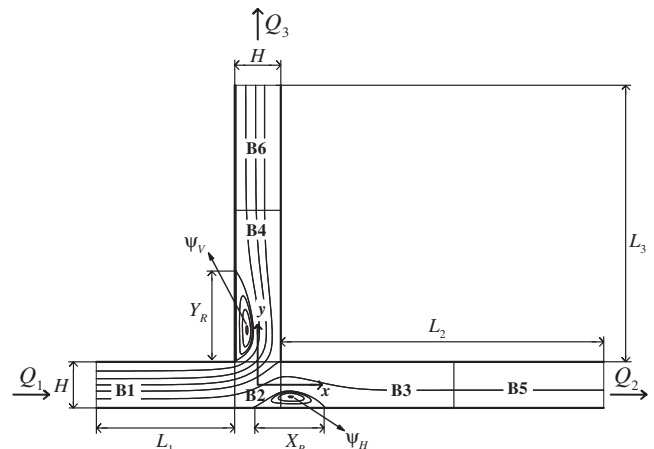


Fig. 1. Bifurcation geometry.

Boundary conditions are prescribed at the inlet and outlet sections, and at the solid walls. At the inlet, placed at section $x = -3.5H$, Dirichlet boundary conditions were used by imposing a parabolic velocity profile valid for laminar steady flows, with mean velocity \bar{u}_1 . At the outlets, located at $x = 22.5H$ and $y = 20.5H$, Neumann boundary conditions were applied, by imposing vanishing axial variations of all variables (i.e. $\partial/\partial x = 0$ in the horizontal duct and $\partial/\partial y = 0$ in the vertical duct), except pressure. Pressure boundary values were obtained by linear extrapolation from the interior followed by forcing overall mass conservation. At the solid walls a no slip boundary condition was imposed, and the stresses were derived from local analytical expressions under simple shear viscometric conditions.

In order to ensure a unique solution of the governing equations in a bifurcation flow it is necessary to apply an extra boundary condition to express the ratio of fluid that flows over each bifurcation channel. This goal could be attained either by enforcing the pressure at the outlets, e.g. [38], or by imposing directly the flow rate ratio (χ) in each arm, the option followed here, where the percentage of fluid in the secondary branch was chosen as reference throughout the text, following Eq. (9d), where Q_1 and Q_3 are respectively the volumetric flow rates at the inlet and at the secondary branch outlet as represented in Fig. 1. Hence $Q_2 = (1 - \chi)Q_1$ is the volumetric flow rate at the main branch outlet. The flow rate ratio was constant for all simulations with $\chi = 0.7$ [18,19]. In hemodynamics applications χ may vary depending on the actual vessel bifurcation considered; for example, Ku et al. [3] mentioned $\chi = 0.7$ for the mean flow rate ratio into the internal carotid, while Gokhale et al. [8] reports values of $\chi = 0.31$ and 0.23 for the celiac and mesenteric bifurcations of the aorta, globally giving a 47% extraction ratio. Therefore in future study χ should be varied parametrically, as in [20] for the Newtonian case and [21] for the GNF Carreau-Yasuda case.

The mesh used is the same to that utilized in past works [21,22], where a study of mesh convergence was presented and is not repeated here. The study was centred on the analysis of the variation of the discretisation error for the horizontal and vertical recirculation length predictions as obtained on several progressively refined meshes. It showed a good proximity between the solutions obtained with the standard mesh and the reference solution obtained through Richardson extrapolation technique, which have resulted in errors less than 2%.

The recirculation lengths X_R and Y_R are identified in Fig. 1. They characterize the bifurcation flow and were obtained through the difference between the reattachment points of the flow, at X_r and Y_r where the recirculation ends, and the separation points of the flow, at X_s and Y_s where the recirculation begins.

5. Results and discussion

In this section we present and discuss the computational results. It is arranged in three subsections: (i) firstly, we analyse the influence of elasticity, through the Deborah number, and the influence of constitutive model; then, we vary systematically the (ii) viscosity ratio β and the (iii) extensibility parameter L^2 , and see how that affects the recirculation eddies. All results are normalised using as length scale the channels height H (that is, $Y = y/H$ and $X = x/H$), as velocity scale the average velocity of the inlet flow (\bar{u}_1), and as stress scale the value of the wall shear stress at inlet, under fully-developed steady flow ($\tau_{w1} = 6\eta_0\bar{u}_1/H$). Both the Reynolds number ($Re = 102$) and the extraction ratio ($\chi \equiv Q_3/Q_1 = 0.70$) are kept constant; these values are the same as in previous studies [17–19,22]. The present study is therefore restricted to variation of constitutive model (FENE-MCR or CR),

Deborah number $De = \lambda\bar{u}_1/H$, viscosity ratio $\beta = \eta_v/\eta_0$ and extensibility of the rheological model L^2 .

5.1. Effect of constitutive model and Deborah number

In this sub-section we focus on the influence of elasticity, as measured by the Deborah number, and additionally we also probe the constitutive model. Elasticity was increased directly by raising the relaxation time (λ) while keeping constant the mean inlet velocity \bar{u}_1 and the channel height H .

Fig. 2 presents the evolution of the horizontal recirculation length with the Deborah number, for two values of the solvent viscosity ratio ($\beta = 0.7$ and 0.8). It is remarked that these particular values of β are typical in hemodynamics (e.g. [4] employed $\beta = 0.9$ in simulations with the Oldroyd-B model; [14] varied β from 0 to 0.9). The results presented also provide a comparison between numerical solutions based on the FENE-CR and the FENE-MCR constitutive models. As shown, both constitutive models predict practically the same values of the horizontal recirculation lengths, as the Deborah number is increased up to a level beyond which iterative convergence can no longer be achieved. In general, the horizontal recirculation length shows a significant decrease with elasticity (of about 16%), starting immediately as the Deborah number is raised above zero (the lower limiting Newtonian case), while for higher values of Deborah number the horizontal recirculation length follows a smoother variation, with a decreasing rate of decay of X_R versus De . However the variation of the eddy size is monotonic over the whole range of De , a feature not observed with the corresponding eddy intensity discussed below (cf. Fig. 5).

The behaviour of the horizontal eddy length and intensity appears more complex than that for the vertical eddy because it depends on the locations of both the separation and the recovery points of the recirculating flow, which vary simultaneously as elasticity is increased, but not always towards the same direction. The spatial displacement of those points with elasticity is illustrated in Fig. 3 for a given case of $\beta = 0.8$, with the two constitutive models (FENE-CR and FENE-MCR) although the variation is similar with both.

At low Deborah numbers both the separation and reattachment points move quickly upstream as elasticity increases, however the rate of variation of the reattachment point is higher and therefore the horizontal recirculation length tends to diminish faster. For Deborah numbers between approximately 1.0 and 2.0 (Fig. 3) the location of the separation point is already increasing (moving towards the outlet), while the reattachment point is still decreasing (moving towards the inlet), thus explaining the localised sharp decrease in the eddy length decay rate observed in Fig. 2 (De just below 1) and increase in eddy intensity observed in Fig. 5. For higher Deborah numbers, the separation moves downstream and the reattachment point moves upstream but at a smaller rate, and consequently leading to recirculation lengths shrinking slowly.

In contrast, the length of the vertical recirculation exhibits a much simpler behaviour because, in this case, the separation point hardly varies with given flow characteristics, since its location is imposed by the geometry. In these circumstances the variation of recirculation length is almost exclusively due to the movement of the recovery point resulting in a monotonous decreasing tendency. Fig. 4 illustrates the variation of the vertical recirculation length with Deborah number for the two constitutive models and shows a consistent shrinkage of the eddy when Deborah number is raised. Two values of viscosity ratio are shown ($\beta = 0.7$ and 0.8) and the reduction in eddy size is markedly higher for the smaller value of β , which is expected since it corresponds to higher dilute-phase concentration and therefore to intensification of elasticity effects.

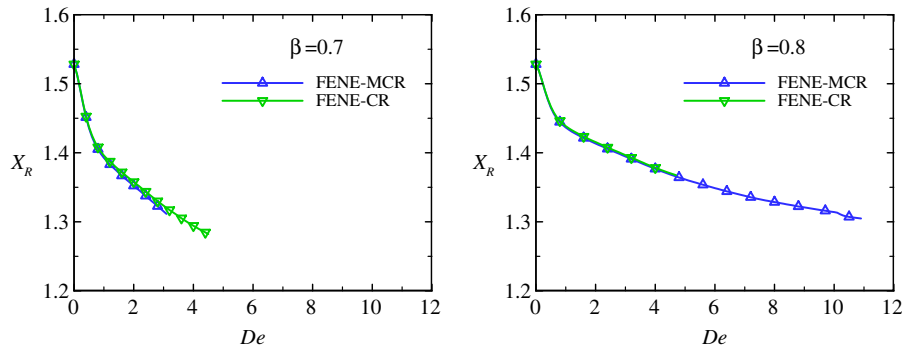


Fig. 2. Variation of the horizontal eddy length (X_R) with the Deborah number (De), for the FENE-MCR and CR models and two values of the viscosity ratio (β).

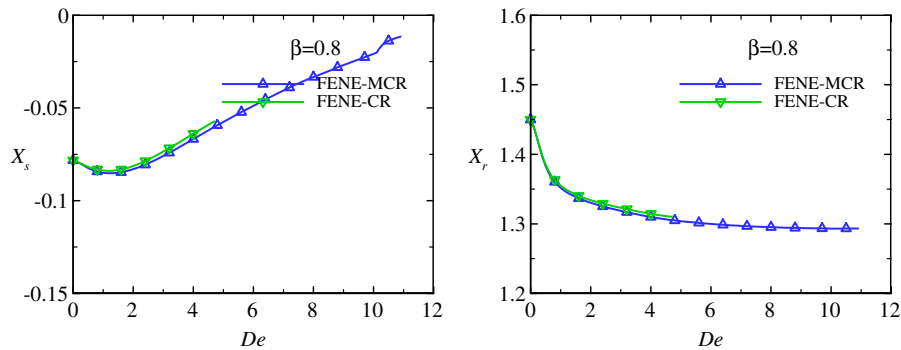


Fig. 3. Movement of the separation (X_s) and reattachment (X_r) points of the horizontal recirculation with the Deborah number (De) for the FENE-CR and MCR models.

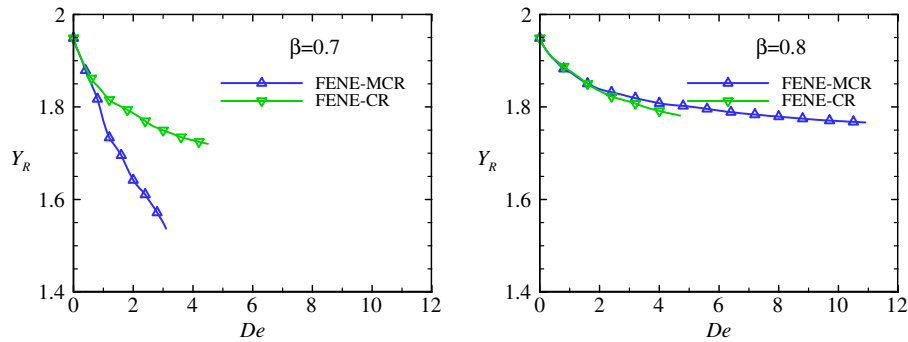


Fig. 4. Variation of the vertical eddy size (Y_R) with the Deborah number (De) for the FENE-MCR and CR models, and for two values of β .

In addition Fig. 4 shows a notorious effect of constitutive model upon the size of the eddy formed in the side branch, in contrast to what occurred for the horizontal eddy where the FENE-MCR and CR yielded almost the same results (cf. Fig. 2). Such occurrence justifies the inclusion in this study of a comparison between CR and MCR models. Differences between the predictions of eddy length produced by the two models can be significant: for example, with $\beta = 0.7$ and $De \cong 3$ there is a 12% difference. These differences must be related to the transient start-up properties of the two models, since a parcel of fluid experiences an important acceleration, with its velocity varying from $v = 0$ at the entrance to the side branch ($y \approx +H/2$), to about $v = \chi 1.5\bar{u}_1$ at a station situated at about the end of the vertical eddy ($y/H \approx Y_R$). We recall that the CR model has a sharper increase of the extensional viscosity upon inception of uniaxial elongational flow as compared to the MCR model. Hence the dumbbell of the CR becomes fully extended very quickly, thus saturating its elasticity, while the MCR dumbbell takes longer

(about twice) to reach steady state in extensional flow, allowing sufficient time for the fluid to go around the vertical eddy in the actual T-junction flow. For an estimated local Weissenberg number of 5 based on an extensional rate evaluated as mentioned above, the time for the elongational viscosity of the CR model to attain its steady state value is about 0.6λ while it is about 1.2λ for the MCR. We hypothesise that the level of stresses is proportional to the strain (and not strain rate) developed, which is larger for the MCR model, resulting in stronger vortex suppression at high elasticity, as seen in Fig. 4 for the lower β . Of course, at steady state (in a Lagrangian sense), the stresses of the two models are the same.

The eddy intensities of the horizontal (ψ_H) and vertical (ψ_V) recirculations are shown in Figs. 5 and 6 respectively. These are calculated from the stream-function field, $u = \partial \psi / \partial y$ and $v = -\partial \psi / \partial x$, with $\psi_H = |\psi_{\min}|$ being the magnitude of the stream function at the eye of the horizontal eddy and thus representing

the amount of fluid in circulation there, in relation to the inlet flow rate, and $\psi_V = \psi_{\max} - 1$ giving the amount of fluid moving in the vertical eddy. Fig. 5 shows that the rheological model (MCR or CR) does not affect the amount of recirculating fluid in the horizontal eddy, which follows a pattern of variation with De having an initial sharp decrease of ψ_H , followed by an intermediate slight increase and a final slower decrease at high De . This behaviour was already discussed when commenting (in relation to Fig. 3) the variation of the separation and reattachment points of the horizontal eddy.

Regarding the vertical recirculation, the vortex strengths obtained with the two constitutive models are slightly different (Fig. 6) and agreement between results is only achieved at relatively low Deborah numbers, as occurred in the analysis of the eddy length variation. The vortex strength behaviour for different constitutive models also depends on the solvent viscosity ratio, with higher vortex strengths inside the recirculating bubble occurring for $\beta \leq 0.7$ when the FENE-MCR model is employed, while for higher values of β the solution for the vortex strength obtained with FENE-CR have larger magnitudes.

Fig. 7 presents the distribution of the total shear stress fields for increasing elasticity, starting from the Newtonian case ($De = 0$) and going up to an elastic case with $De = 3$. For viscoelastic fluids the total shear stress is obtained by the sum of viscoelastic (or polymer-like) and Newtonian (or solvent-like) stress components, with the solvent component having a weight of β and presenting a stress distribution identical to that for the corresponding Newtonian case at the same Reynolds number. Since there are only minor differences in contour plots between the shear stress results from the FENE-MCR and the FENE-CR models, only the latter results are shown.

Fig. 7 shows the influence of elasticity upon the total (viscoelastic plus Newtonian) shear stress fields, using the FENE-CR model

and the same solvent viscosity ratio as before ($\beta = 0.7$). It also separates the Newtonian and viscoelastic contributions for the particular value of $De = 1$. In general elasticity promotes an increase in the gradients of the viscoelastic part of the shear stress, with their values tending to increase in modulus over the entire flow domain. Noticeable features in Fig. 7 and in corresponding plots of the viscoelastic component of the stress (shown only for $De = 1$) are the development of positive shear layers from the elasticity-inducing dispersed phase contribution over the recirculation vortices found in the lower side of the horizontal channel and the upstream side of the vertical side arm. In particular, this tendency becomes more intense as De is raised, and positive values of $\tau_{xy,V}$ are retained extending up to the vertical position of the eye of the vertical recirculation.

As shown in parts c and d of Fig. 7 (the middle row), the sign of the viscoelastic shear stresses near the re-entrant corner is opposite to that for the Newtonian component. It is also possible to confirm the proximity between the pure Newtonian case and Newtonian shear stress fields. The Newtonian shear stress contributes in a larger proportion than the viscoelastic component to the total shear stress over the whole domain, a first conclusion that partly results from having here $\beta = 0.7$, and a second conclusion is that the extreme stress values are mainly located in the bifurcation zone. With exception of the area adjacent to the first (upstream) re-entrant corner, the signs of the shear stresses for both stress contributions (Newtonian and viscoelastic) are locally the same, resulting in a shear stress increase with Deborah number over the whole domain, as it may be observed in the sequence of plots for varying De in Fig. 7.

However, at the upstream re-entrant corner ($Y = +0.5$ and $X = -0.5$), although the Newtonian and viscoelastic shear stress contributions have opposite signs, we observe that, since the latter is much higher at this location, the Newtonian contribution is min-

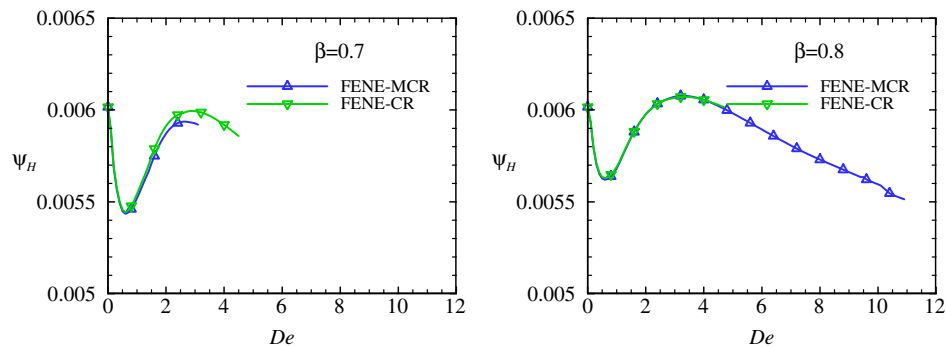


Fig. 5. Variation of the horizontal recirculation eddy intensity (ψ_H) with the Deborah number (De).

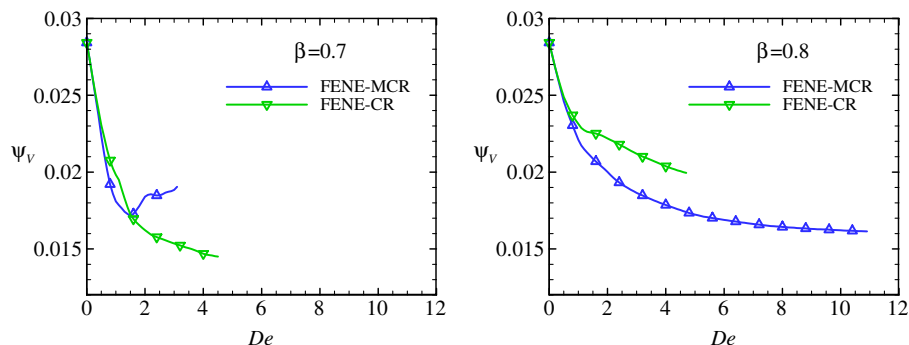


Fig. 6. Variation of the vertical recirculation eddy intensity (ψ_V) with the Deborah number (De).

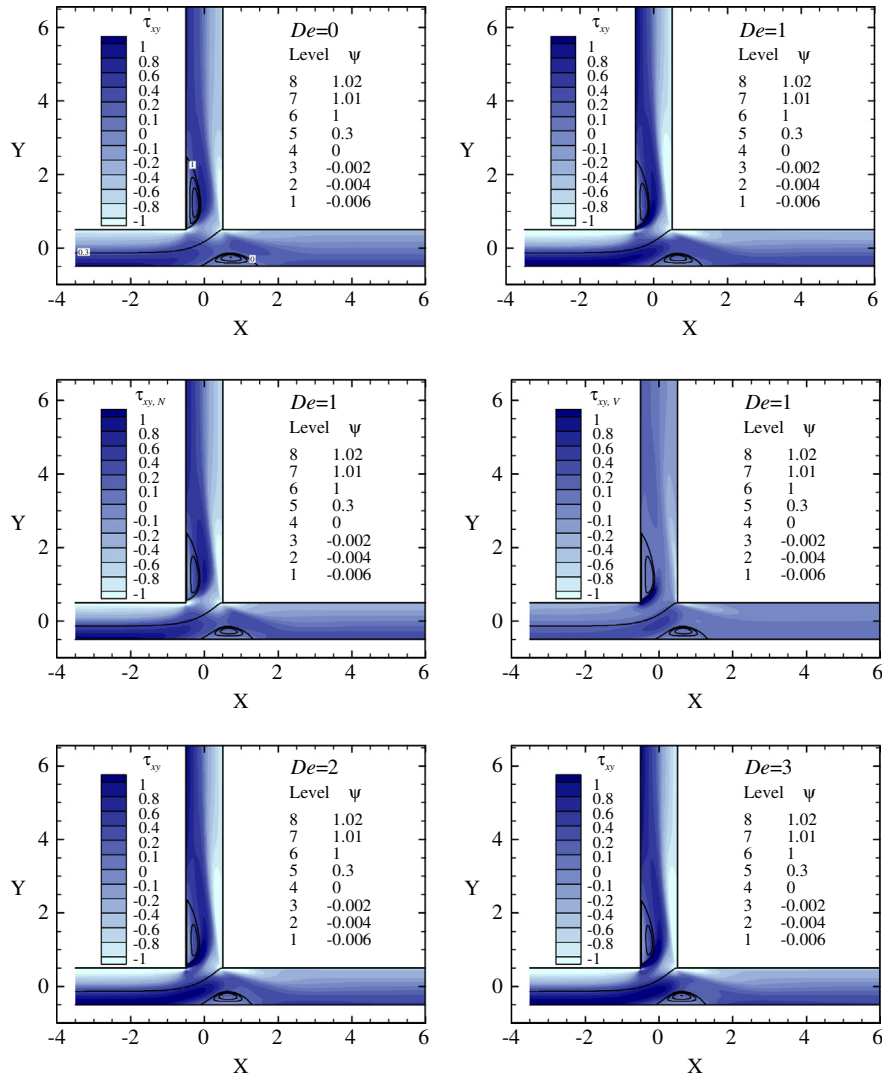


Fig. 7. Shear stress contours for various Deborah numbers at $\beta = 0.7$ with the FENE-CR model. Newtonian and viscoelastic stress components ($\tau_{xy,N}$ and $\tau_{xy,V}$) shown for the case $De = 1$.

imised. For this particular case with $De = 1$ the maximum and minimum registered shear stresses are $\tau_{xy,max} = 1.09$ and $\tau_{xy,min} = -4.31$ for the Newtonian contribution, and $\tau_{xy,max} = 6.66$ and $\tau_{xy,min} = -5.35$ for the viscoelastic contribution.

As elasticity is raised the shear stress gradients become more intense, encircling the zones where the maximum and minimum shear stresses are located. Maximum shear stresses follow the streamlines having $\psi = 0$ and $\psi = 1$, and are located along the horizontal bottom wall and the vertical left wall, with exception of the recirculation zones where they tend to follow the eddy boundary. The maximum magnitudes of τ_{xy} occur at the first re-entrant corner, the location from which the vertical recirculation starts. On the other hand the minimum shear stresses occur along the horizontal top wall and the vertical right wall, with smallest magnitudes at the second (downstream) re-entrant corner.

Shear stresses inside the recirculation zones tend to be very low in absolute value, a feature better observed in contour plots of $|\tau_{xy}|$, as shown in Fig. 8 for $De = 3$, where two scales are employed, with lower magnitudes more clearly identified on the right plot. In the Introduction it was pointed out that rather than the presence of extreme values of shear stress, it is the generation of large spatial/temporal shear stress gradients which is nowadays

favoured as an explanation for the initiation and development of the atherosclerotic disease.

Fig. 8 shows that at the beginning and at the end of the two recirculating eddies formed by the channel bifurcation the shear stress gradients are considerable, a factor that would tend to promote the occurrence of atherosclerotic disease close to recirculation zones, in the particular case of hemodynamical applications.

In addition to the stress contour plots of the previous figures, it is useful to look at the actual stresses acting on the T-junction walls. Shear stress profiles along the lower ($y = -0.5H$) and upper ($y = +0.5H$) walls of the main channel, and the upstream ($x = -0.5H$) and downstream ($x = +0.5H$) walls of the lateral side channel are shown in Fig. 9 for a typical value of $\beta = 0.7$ and various values of Deborah number, ranging from $De = 0$ (Newtonian case) to $De = 3$ (highly elastic). In particular, this comparison clarifies that although the total shear stress is the same under fully developed flow, irrespective of Deborah number, there is a tendency for larger stresses (in modulus) near the points of intersection of the side and the main channels as De is raised. For the vertical channel walls, elasticity induces large peaks of shear stress, both positive τ_{xy} (upstream wall) and negative τ_{xy} (downstream wall), lasting for about a distance of 0.25 channel widths.

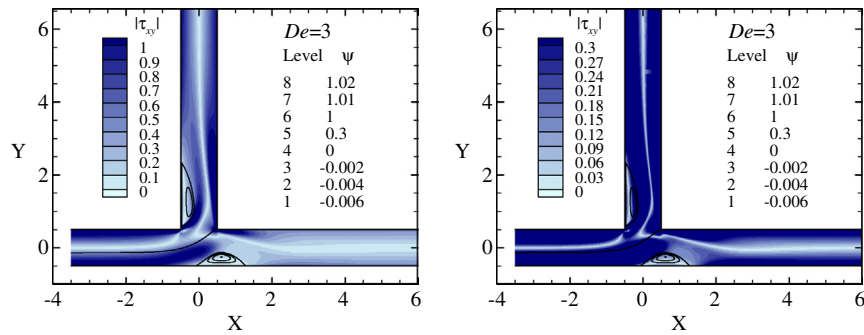


Fig. 8. Contour plot of shear stress modulus for the case $De = 3$ and $\beta = 0.7$, with the FENE-CR model. The right figure highlights lower magnitudes of absolute stress values.

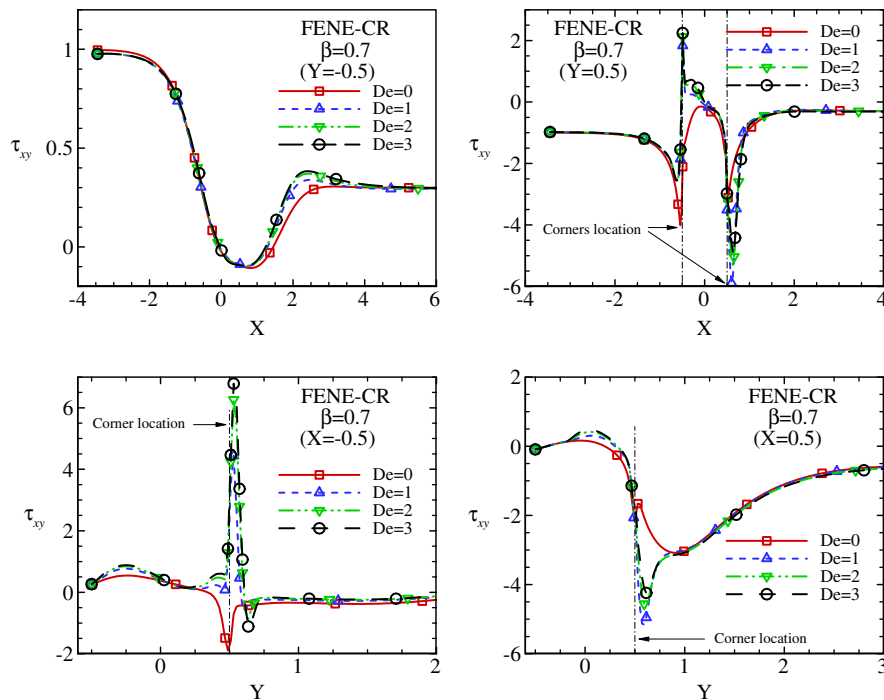


Fig. 9. Profiles of shear stress along the walls of the horizontal and vertical channels.

5.2. Effect of the concentration parameter

The present subsection deals with the influence of viscosity ratio upon the main vortex characteristics. For the case of blood flow β should be constant but its exact value is uncertain and therefore a study of its parametric influence is worth pursuing. Leuprecht and Perktold [4], for example, considered a relaxation time of 0.06 s and a retardation time of 0.054 s giving $\beta = 0.9$, in their simulations with an Oldroyd-B model. It is remarked that a decrease of β corresponds to increased dispersed-phase concentration as implied by the definition of Eq. (9c) and therefore the resulting liquid mixture solution will show higher elasticity. For example, for the limiting case of the Oldroyd-B model, normal stress effects including the influence of elastic-phase concentration lead to a modified Deborah number $De_{\text{mod}} = (1 - \beta)De$.

We note that for the present case, the above relaxation time for blood would correspond to a Deborah number of $De = 0.45$; typical De in hemodynamics may rise to 2–5 for higher blood velocities and differing conditions. Actual Deborah numbers calculated on the basis of the arterial data provided by Wootton and Ku [39], using $\lambda = 0.06$ s (also mentioned by Gijzen et al. [10]; other authors refer higher blood relaxation times, e.g. $\lambda = 0.145$ s in Owens [7], or

$\lambda = 0.3$ s in Chakraborty et al. [15] and Gijzen et al. [9] for a blood analog fluid; however, [5] refers a lower value, $\lambda = 0.017$ s), give $De = \lambda \bar{u}/R = 4.5$ for the femoral artery, $De = 3.8$ for the common carotid and $De = 6.9$ for the left main coronary. These values are in the range here considered, as well as in other studies (e.g. [14] varied De from 0 to 3).

Figs. 10 and 11 show, respectively, the changes in the horizontal and vertical recirculation lengths brought about by increasing De and decreasing the viscosity ratio β , for the FENE-CR constitutive model. The data are plotted as a function of simply De (left side) or of the modified Deborah number De_{mod} (right side).

Both figures show a strong shrinking of the recirculation eddies as elasticity is enhanced by raising the dispersed-phase viscoelastic-inducing concentration (inversely proportional to β), which is monotonic with De and β for both the horizontal eddy (Fig. 10) and the vertical eddy (Fig. 11). There is a certain tendency for collapsing the data by using the modified Deborah number, which is more accentuated at lower De and smaller β . Perfect data collapsing was however not expected for a complex flow, as the present one, and for a finitely extensible dumbbell model.

When β is raised, the plots on the left side of Figs. 10 and 11 show that converged solutions are achieved for much higher

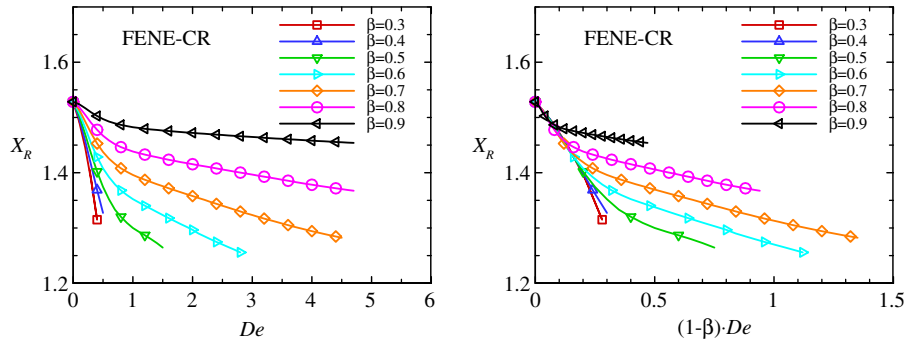


Fig. 10. Parametric variation of the horizontal eddy size (X_R) with the viscosity ratio (β).

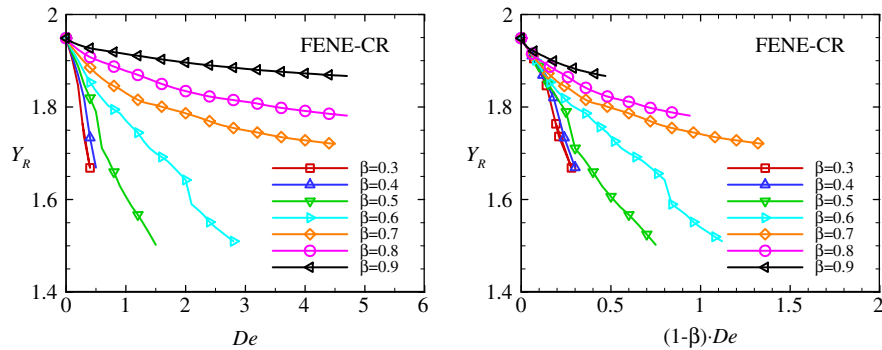


Fig. 11. Parametric variation of the vertical eddy size (Y_R) with the viscosity ratio (β).

Deborah numbers ($De_{\max} \approx 4.5$ for $\beta \approx 0.7, 0.8$ and 0.9 , compared to $De_{\max} \approx 0.5$ for $\beta \approx 0.3$ and 0.4), reflecting the more diffusive nature of the flow as the stress becomes closer to a pure Newtonian stress. In the present calculations the time step was maintained fixed ($\Delta t \approx 0.01$ (scaled with H/\bar{u}_1)) and we have not explored the possibility of testing smaller Δt so as to extend the range of allowable De . Anyway, it is well known that sharp re-entrant corners pose a severe test to viscoelastic calculations because the stresses tend to rise quickly to infinity at those singular points. In hemodynamical applications these corners are of course rounded and the angle of the diverting channel to the main channel is not 90° , two factors which tend to attenuate those convergence problems of viscoelastic computations.

Horizontal vortex intensity varies with viscosity ratio in a more complex way compared to vortex size, as shown for the horizontal recirculation in Fig. 12, which exhibits again a non-monotonous behaviour with the Deborah number but monotonous with the viscosity ratio: at low Deborah numbers there is the expected vortex

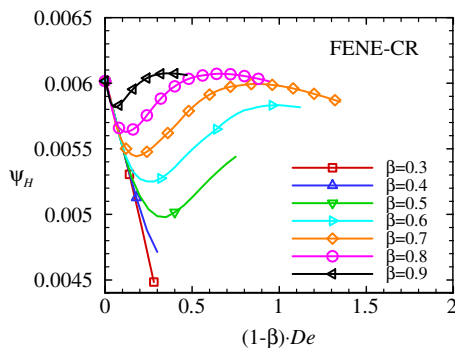


Fig. 12. Horizontal eddy intensity (ψ_H) as a function of viscosity ratio (β) and modified Deborah number (De_{mod}) (FENE-CR model).

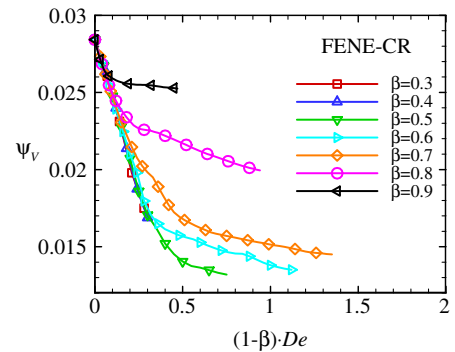


Fig. 13. Vertical eddy intensity (ψ_V) as a function of viscosity ratio (β) and modified Deborah number (De_{mod}) (FENE-CR model).

attenuation with elasticity as β is reduced (and viscoelastic-phase concentration increased); at higher De values the degree of attenuation is reduced or almost vanishes (an indication of saturation of the dumbbell extensibility of the model).

For the vertical recirculation, however, the vortex intensity follows a monotonic variation with both De and β (Fig. 13), generally showing strong attenuation by elasticity. Magnitudes of vortex strength are in this case much higher compared to the values registered for the horizontal recirculation, for all viscosity ratios, because the change in fluid trajectory at 90° on entering the secondary branch favours the inception of eddy formation and development, compared with horizontal recirculation. In the vertical eddy, intensity attains about 3% of the incoming flow rate while the horizontal eddy has intensities of about 0.6%. However the decay of intensity of the vertical eddy attains almost a factor of 2, from 3% to 1.5% when $\beta = 0.5$, while the corresponding eddy size is only reduced by elasticity by about $0.35/1.9 \approx 18\%$. Since this

eddy is more clearly controlled by elasticity, there is a better agreement between the various sets of data when these are plotted as a function of the modified Deborah number, especially in the middle range of β ($\beta \cong 0.5$ – 0.7).

An interesting feature common to both sets of Figs. 12 and 13, for the eddy intensity, and Figs. 10 and 11 for the eddy size, is that the decay of these quantities is almost linear at low De_{mod} . Such behaviour, generally indicating immediate vortex suppression and attenuation with minor elasticity, could be explained by an asymptotic tendency in the linear viscoelastic limit.

Contour plots of the total shear stress field would show that the stresses tend to decrease in size when the viscosity ratio is increased, very similar to the effect of increasing De seen in Fig. 7, and so, for conciseness, those contours are not given here. Locations with very high shear stresses in modulus are found near the re-entrant corners and around the recirculation boundaries, while the inside of the recirculation zones is characterized by very low shear stresses in modulus near the wall. To permit a more quantitative assessment of stress levels, the variations of the predicted maximum and minimum shear stress values with Deborah number and solvent viscosity ratio are plotted in Fig. 14.

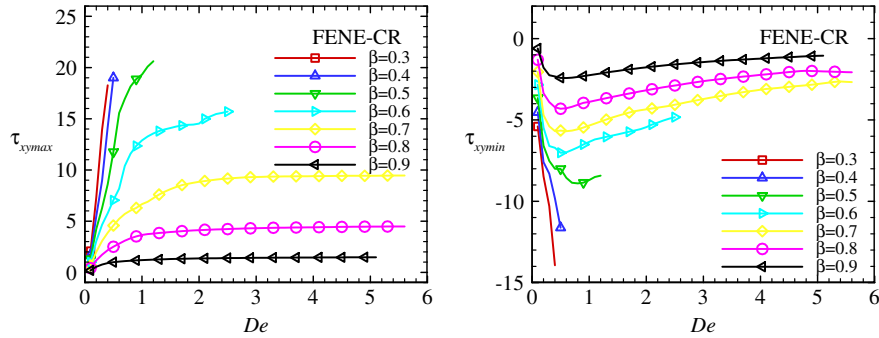


Fig. 14. Values of maximum and minimum shear stress for varying De and β (FENE-CR model).

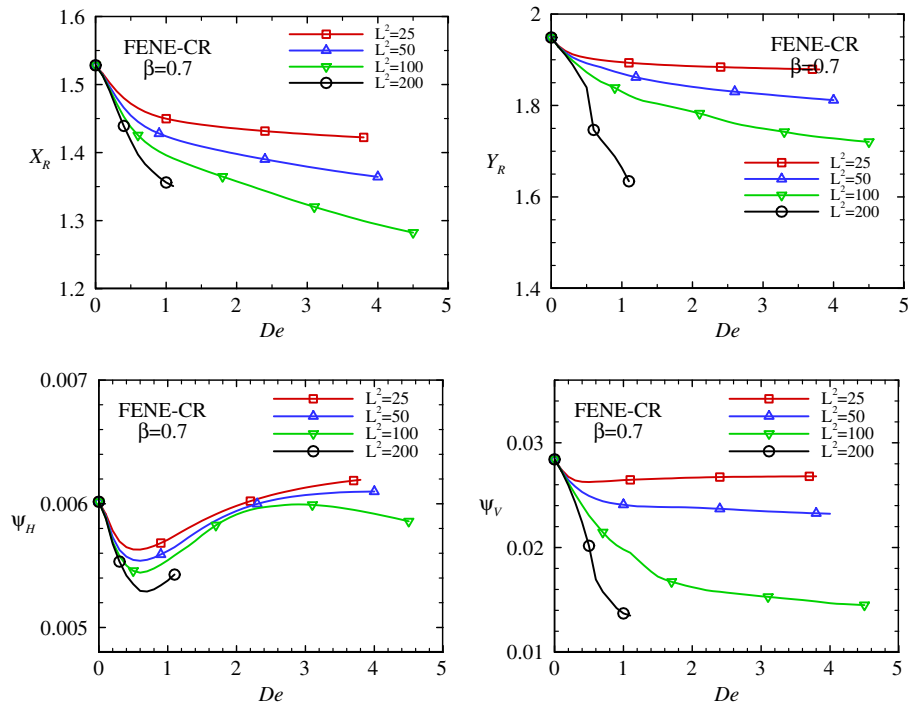


Fig. 15. Effect of extensibility parameter L^2 upon the vortex sizes (upper row) and intensities (lower row), FENE-CR model with $\beta = 0.7$.

Fig. 14 shows that the highest values of shear stress, which are registered in the re-entrant corners, can be 20 times higher than the wall shear stress at the inlet, especially for the simulations with small β ($\beta \leq 0.5$). When comparing the maximum stress values from the two constitutive models, it may be concluded that the FENE-MCR model gives much higher values than the FENE-CR, especially as β is decreased. A reason for this was discussed above, in relation with Fig. 4. The maximum and minimum shear stresses also increase in modulus with Deborah number and inversely with Newtonian to total viscosity ratio, in agreement with the shear stress field variation analysed above.

5.3. Effect of extensibility parameter

In the previous subsections all results were obtained for the base value of $L^2 = 100$. Although that is a common value for the extensibility parameter in various studies with FENE-P and FENE-CR models, ranging from fundamental investigations of cross-slot flows to contraction and expansion flows, but also including hemodynamics applications as those of [14,15], we have here probed the parametrical influence of varying L^2 around that base value.

Fig. 15 illustrates the variation of the horizontal and vertical eddy sizes, upper row, and the corresponding eddy intensities, lower row. These results were obtained for the specific viscosity ratio of $\beta = 0.7$, also used in Section 5.1, and for L^2 taking the values of 25, 50, 100 and 200. We recall that large values of L^2 make the FENE-CR model tend to the Oldroyd-B model (infinite dumbbell extension) and low values of L^2 have been used in the past, by other authors, to represent polymer melts and also to procure a match between experiments and simulations of FENE models against polymer solution behaviour.

Regarding eddy size, Fig. 15 shows that the horizontal eddy is decreased proportionally to an increase of L^2 , while the vertical eddy has a more dramatic rate of size reduction when extensibility is increased. For the highest value of $L^2 = 200$, it is more difficult to perceive the trends since converged results are restricted to a much narrower range of Deborah number (typically $De \leq 1$). In terms of eddy strength, the horizontal eddy seems little affected by L^2 , although a monotonous tendency for a reduction of eddy intensity is clearly perceived from the data, while the vertical eddy activity follows the same trend seen for the eddy size: when L^2 is raised from 50 to 100 the rate of eddy intensity attenuation is much larger than when L^2 goes from 25 to 50.

So, in conclusion, the larger the extensibility parameter, the smaller and less intense become the two eddies formed at the T-junction, with the eddy formed in the lateral arm being more strongly affected by an increase of L^2 .

6. Conclusions

Numerical simulations were conducted for two-dimensional viscoelastic flow through a planar T-junction. The fluids followed rheological constitutive models of the differential rate-type, but having constant shear viscosity so as to isolate effects due to viscoelasticity (the FENE-CR and FENE-MCR models). The objective of this study was to investigate the influence of elasticity, through variation of the Deborah number and the viscosity ratio, a model parameter which bears a strong relation to the dispersed phase concentration in a liquid mixture, upon steady flows in an 90-degree bifurcation geometry. A relation with hemodynamical flows was set out in the Introduction, especially those linked with the triggering of vascular diseases and atherosclerosis. The occurrence of atherosclerotic plates is frequently related to the existence of flow separation and recirculation regions, where the shear stresses close to the arterial walls possesses high gradients and strong variations. Therefore the main flow parameters under study here, even if the present fluid model is not totally adequate to faithfully represent actual blood flow behaviour, were the lengths of the eddies formed at the junction and the vortex recirculation strengths, and shear stress fields.

A comparison between the rheological models leads to the conclusion that, in terms of numerical behaviour, for the majority of the viscosity ratios the FENE-CR model proved to be more robust (allowing solution at higher De), while for viscosity ratios near unity ($\beta = 0.8$ and $\beta = 0.9$) the FENE-MCR model presents an extended range of Deborah solutions. The predictions of recirculation length and vortex strength for the horizontal recirculation are quite similar with both models. On the other hand, for the vertical recirculation agreement is found only in a relatively low Deborah number range. At high Deborah numbers, two distinct behaviours were registered: for $\beta \leq 0.7$ the FENE-CR model produces longer vertical recirculation and lower vortex strengths in relation to the FENE-MCR, while for larger viscosity ratios the opposite behaviour occurs.

In general, the shear stress fields predicted with both constitutive models do not present significant differences, however in the

re-entrant corners where the shear stresses attain extreme values (positive and negative) there are significant differences between the models, with higher gradients when the FENE-MCR model is applied. For very low solvent viscosity ratios (high elastic effects) the shear stress near the corners predicted with the FENE-CR model may reach 20 times the wall shear stress at inlet.

Regarding the vortex characteristics, a general conclusion is that an increase in elasticity, either by increasing the Deborah number, by decreasing the viscosity ratio, or increasing the extensibility parameter of the dumbbell model, results in a decrease of the size and intensity of the recirculation eddies formed by the junction. The only exception to this behaviour occurs for the vortex intensity of the horizontal recirculation, which shows a non-monotonous variation due to the additional degree of freedom introduced by the displacement of the separation point.

A quantification of the vortex suppression by elasticity shows reduction in vortex size of 16.3% at $\beta = 0.7$, 15.0% at $\beta = 0.8$, and 6.5% at $\beta = 0.9$, for the horizontal eddy at the highest De attained, and 23.1% at $\beta = 0.6$ ($De = 3$), 11.3% at $\beta = 0.7$, and 8.2% at $\beta = 0.8$ (both at $De = 4$), for the vertical eddy. The reduction in vortex intensity, for the vertical eddy, is 10.5% at $\beta = 0.9$, which rises to 50.8% at $\beta = 0.5$ (both at $De = 2$).

On the other hand the shear stress field shows a tendency to increase in modulus with Deborah number, especially due to the intensification of the viscoelastic contribution to the stress. Elasticity also promotes the existence of larger shear stress gradients. Hence, when these results are extended to blood flow, there is an increase of the forces that endothelial cells are subjected to at the artery walls, for an equivalent hemodynamical situation.

A tentative to combine the influences of elasticity through the Deborah number and the viscosity ratio, into a single modified number ($De_{mod} = (1 - \beta)De$), shows some degree of correlation when the eddy length and intensity are plotted versus De_{mod} , which is more successful at higher elasticity (low β) and more effective for the vertical eddy characteristics. In fact, this way of presenting the data suggests a separation between high-elastic and low-elastic flows, separated by $\beta \approx 0.6$, with a more intense suppression of eddy activity for the former case (low β). The fact that this is more clearly seen for the vertical recirculation is explained by the extra degree of freedom introduced by the movement of the separation point in the case of the horizontal recirculation, which also explains the non-monotonic behaviour of the horizontal eddy intensity: at first, there is reduction with De_{mod} , followed by an increase and, eventually, a final decrease.

While the present study has only considered steady viscoelastic flow through a T-junction, a forthcoming paper will address the corresponding unsteady flow case, with attention focussed on the changes induced by unsteadiness and viscoelasticity on the eddy parameters.

Acknowledgments

The authors gratefully acknowledge the financial support conceded by Fundação para a Ciência e a Tecnologia (FCT, Portugal) and COMPETE, under grant SFRH/BD/18062/2004 (Dr. H.M. Matos) and mainly under project PTDC/EME-MFE/098558/2008.

References

- [1] D.P. Giddens, C.K. Zarins, S. Glagov, The role of fluid mechanics in the localization and detection of atherosclerosis, *J. Biomech. Eng.* 115 (1993) 588–594.
- [2] C.G. Caro, J.M. Fitz-Gerald, R.C. Schroter, Atheroma and arterial wall shear. Observation, correlation and proposal of a shear dependent mass transfer mechanism for atherogenesis, *Proc. R. Soc. Lond. B. Biol. Sci.* 177 (1971) 109–159.

- [3] D.N. Ku, D.P. Giddens, C.K. Zarins, S. Glagov, Pulsatile flow and atherosclerosis in the human carotid bifurcation. Positive correlation between plaque location and low oscillating shear stress, *Arteriosclerosis* 5 (1985) 293–302.
- [4] A. Leuprecht, K. Perktold, Computer simulation of non-Newtonian effects on blood flow in large arteries, *Comput. Methods Biomech. Biomed. Eng.* 4 (2001) 149–163.
- [5] M. Brust, C. Schaefer, R. Doerr, L. Pan, M. Garcia, P.E. Arratia, C. Wagner, Rheology of human blood plasma: viscoelastic versus Newtonian behavior, *Phys. Rev. Lett.* 110 (2013) 078305.
- [6] G.B. Thurston, Rheological parameters for the viscosity viscoelasticity and thixotropy of blood, *Biorheology* 16 (1979) 149–162.
- [7] R.G. Owens, A new microstructure-based constitutive model for human blood, *J. Non-Newtonian Fluid Mech.* 140 (2006) 57–70.
- [8] V.V. Gokhale, R.I. Tanner, K.B. Bischoff, Finite element solution of the Navier–Stokes equations for two-dimensional steady flow through a section of a canine aorta model, *J. Biomech.* 11 (1978) 241–249.
- [9] F.J.H. Gijzen, F.N. Van de Vosse, J.D. Janssen, The influence of the non-Newtonian properties of blood on the flow in large arteries: steady flow in a carotid bifurcation model, *J. Biomech.* 32 (1999) 601–608.
- [10] F.J.H. Gijzen, F.N. Van de Vosse, J.D. Janssen, The influence of the non-Newtonian properties of blood on the flow in large arteries: unsteady flow in a 90° curve, *J. Biomech.* 32 (1999) 705–713.
- [11] W.M. Phillips, S. Deutsch, Toward a constitutive equation for blood, *Biorheology* 12 (1975) 383–389.
- [12] Md.A. Ikbal, S. Chakravarty, Sarifuddin, P.K. Mandal, Unsteady analysis of viscoelastic blood flow through arterial stenosis, *Chem. Eng. Commun.* 199 (2011) 40–62.
- [13] K.K. Yeleswarapu, M.V. Kamenewa, K.R. Rajagopal, J.F. Antaki, The flow of blood in tubes: theory and experiment, *Mech. Res. Commun.* 25 (1998) 257–262.
- [14] T. Bodnar, A. Sequeira, M. Prosi, On the shear-thinning and viscoelastic effects of blood flow under various flow rates, *Appl. Math. Comput.* 217 (2010) 5055–5067.
- [15] D. Chakraborty, M. Bajaj, L. Yeo, J. Friend, M. Pasquali, J.R. Prakash, Viscoelastic flow in a two-dimensional collapsible channel, *J. Non-Newtonian Fluid Mech.* 165 (2010) 1204–1218.
- [16] D. Liepsch, S. Moravec, A.K. Rastogi, N.S. Vlachos, Measurement and calculations of laminar flow in a ninety degree bifurcation, *J. Biomech.* 15 (1982) 473–485.
- [17] J.M. Khodadadi, T.M. Nguyen, N.S. Vlachos, Laminar forced convective heat transfer in a two-dimensional 90° bifurcation, *Numer. Heat Transfer* 9 (1986) 677–695.
- [18] J.M. Khodadadi, N.S. Vlachos, D. Liepsch, S. Moravec, LDA measurements and numerical prediction of pulsatile laminar flow in a 90-degree bifurcation, *J. Biomech. Eng.* 110 (1988) 129–136.
- [19] J.M. Khodadadi, Wall pressure and shear stress variations in a 90-Deg bifurcation during pulsatile laminar flow, *J. Fluids Eng.* 113 (1991) 111–115.
- [20] A.I.P. Miranda, P.J. Oliveira, F.T. Pinho, Steady and unsteady laminar flows of Newtonian and generalized Newtonian fluids in a planar T-junction, *Int. J. Numer. Meth. Fluids* 57 (2008) 295–328.
- [21] H.M. Matos, P.J. Oliveira, Steady and unsteady non-Newtonian inelastic flows in a planar T-junction, *Int. J. Heat Fluid Flow* 39 (2013) 102–126.
- [22] H.M. Matos, M.A. Alves, P.J. Oliveira, New formulation for stress calculation: application to viscoelastic flow in a T-junction, *Numer. Heat Transfer B-Fund.* 56 (2009) 351–371.
- [23] A. Soleymani, H. Yousefi, I. Turunen, Dimensionless number for identification of flow patterns inside a T-micromixer, *Chem. Eng. Sci.* 63 (2008) 5291–5297.
- [24] F. Bianchi, R. Ferrigno, H.H. Girault, Finite element simulation of an electroosmotic-driven flow division at a T-junction of microscale dimensions, *Anal. Chem.* 729 (2000) 1987–1993.
- [25] J.S. Anagnostopoulos, D.S. Mathioulakis, Unsteady flow field in a square tube T-junction, *Phys. Fluids* 16 (2004) 3900–3910.
- [26] R.J. Poole, M. Alfateh, A.P. Gauntlett, Bifurcation in a T-channel junction: Effects of aspect ratio and shear-thinning, *Chem. Eng. Sci.* 104 (2013) 839–848.
- [27] J. Soulaes, M.S.N. Oliveira, P.C. Sousa, M.A. Alves, G.H. McKinley, Investigating the stability of viscoelastic stagnation flows in T-shaped microchannels, *J. Non-Newtonian Fluid Mech.* 163 (2009) 9–24.
- [28] R.B. Bird, O. Hassager, R.C. Armstrong, C.F. Curtiss, *Dynamics of Polymeric Liquids: Kinetic Theory*, vol. II, John Wiley & Sons, 1987.
- [29] M.D. Chilcott, J.M. Rallison, Creeping flow of dilute polymer solutions past cylinders and spheres, *J. Non-Newtonian Fluid Mech.* 29 (1988) 381–432.
- [30] P.J. Coates, R.C. Armstrong, R.A. Brown, Calculation of steady state viscoelastic flow through axisymmetric contractions with the EEME formulation, *J. Non-Newtonian Fluid Mech.* 42 (1992) 141–188.
- [31] X. Huang, N. Phan-Thien, R.I. Tanner, Viscoelastic flow between eccentric rotating cylinders: unstructured control volume method, *J. Non-Newtonian Fluid Mech.* 64 (1996) 71–92.
- [32] J.P. Van Doormaal, G.D. Raithby, Enhancements of the SIMPLE method for predicting incompressible fluid flows, *Numer. Heat Transfer* 7 (1984) 147–163.
- [33] P.J. Oliveira, F.T. Pinho, G.A. Pinto, Numerical simulation of non-linear flows with a general collocated finite-volume method, *J. Non-Newton Fluid Mech.* 79 (1998) 1–43.
- [34] R.I. Issa, P.J. Oliveira, Numerical prediction of phase-separation in two-phase flow through T-junctions, *Comput. Fluids* 23 (1994) 347–372.
- [35] P.J. Oliveira, F.T. Pinho, Numerical procedure for the computation of fluid flow with arbitrary stress–strain relationships, *Numer. Heat Transfer B-Fund.* 35 (1999) 295–315.
- [36] M.A. Alves, P.J. Oliveira, F.T. Pinho, A convergent and universally bounded interpolation scheme for the treatment of advection, *Int. J. Numer. Meth. Fluids* 41 (2003) 47–75.
- [37] R.K. Shah, A.L. London, *Laminar flow forced convection in ducts*, Supplement 1 to *Advances in Heat Transfer*, Academic Press, New York, 1978.
- [38] N. Moshkin, D. Yambangwi, Steady viscous incompressible flow driven by a pressure difference in a planar T-junction channel, *Int. J. Comput. Fluid Dyn.* 23 (2009) 259–270.
- [39] D.M. Wootton, D.N. Ku, Fluid mechanics of vascular systems, diseases, and thrombosis, *Annu. Rev. Biomed. Eng.* 01 (1999) 299–329.